STATIC LOAD MODELING DURING LARGE FREQUENCY FLUCTUATIONS: AN EXPERIMENTAL INVESTIGATION WITH INDIVIDUAL DEVICES

***Johanna Geis-Schroer*[1*], *Gregor Bock*[1], *Qiucen Tao*[2]**
***Michael Suriyah*[1], *Giovanni De Carne*[2], *Thomas Leibfried*[1]**

Karlsruhe Institute of Technology (KIT), Karlsruhe, Germany
[1]*Institute of Electric Energy Systems and High-Voltage Technology (IEH)*
[2]*Institute for Technical Physics (ITEP)*
[*]*johanna.geis-schroer@kit.edu*

Keywords: LOAD MODELING, FREQUENCY DEPENDENCY, POWER ELECTRONIC-INTERFACED LOADS

Abstract

In the past, frequency dependency has often been neglected in load modeling. However, the volatility of frequency is likely to increase in future grid scenarios. To assess novel strategies to increase flexibility in distribution grids, it becomes crucial to accurately model the power response of connected loads to larger frequency fluctuations. The experimental study presented in this paper aims to provide insights into the load behavior of modern load devices in the range 50±6 Hz. The three devices under test represent commonly used load technologies in low-voltage grids. For active and reactive power of each device, we identify three static load models based on steady-state measurements; a lookup table model as a result of interpolation, as well as an exponential model and a linear model based on curve fitting. Then, we assess whether these models can reconstruct the behavior of the devices during dynamic frequency variations. When comparing the measured and reconstructed power, we find the largest deviations for the motor-based load under test. For the power electronic-interfaced load under test, we observe that reactive power is significantly more frequency-dependent than active power. The outcomes of our study can be helpful for novel demand-side management strategies such as frequency-based power control.

1 Introduction

Accurately representing the characteristics of connected loads is essential for the successful examination of distribution system planning, operation and control strategies. Both for steady-state and dynamic power system studies, European distribution grid operators predominantly use static load models [1]. Numerous static load models for different types of individual and aggregate loads can be found in the literature [2, 3]. However, the key difference in these models lies in the representation of power-to-voltage dependency. In past research, little attention has been given to frequency-dependent load behavior. This can be attributed to the fact that, except for a limited number of remote island systems, European distribution grids are synchronously connected to large interconnected transmission networks. Hence, frequency deviations tend to be small compared to voltage deviations.

With increasing penetration of power electronic-based generation from renewable resources, we can expect frequency to become more volatile in future grid scenarios [4]. This calls for a closer investigation into the frequency-dependent behavior of connected loads. Improved understanding of this subject is also crucial for assessing novel strategies to enhance flexibility in distribution grids. For instance, one of the options currently being researched is frequency-based power control in asynchronously connected low-voltage grids [5, 6]. By means of the measurement-based approach presented in this contribution, we aim at providing insights into the frequency-dependent active and reactive power characteristics of three exemplary load devices of different technology. Our study considers both steady-state and dynamic frequency deviations in the range 50±6 Hz. This range is in alignment with frequency disturbances to which loads may already be exposed in some remote European island systems today [7].

The rest of this paper is structured as follows: Section 2 summarizes the state-of-the-art representation of power-to-frequency dependency in static load models. Section 3 introduces the devices under test, and outlines our experimental methodology used to analyze their frequency-dependent load behavior. The results are presented and discussed in Section 4. Finally, Section 5 concludes with a summary and suggestions for future work.

2 State of the art

Static load models describe the active and reactive power consumed by a load as simple functions of the voltage magnitude and frequency at the load bus. Two approaches to consider frequency dependency are reported in the literature [2, 3]: A voltage-dependent term (e.g. voltage-dependent exponential or polynomial model) is multiplied by a linear or an exponential frequency-dependent term. In this paper, we only focus

on frequency dependency, i.e. the voltage is maintained at the nominal value (see Section 3.2). The voltage-dependent term can thus be neglected. The two approaches can be summarized as defined in (1) and (2), where P_0 is the active power consumed at the rated frequency f_0. Each model has a single unknown parameter: $k_{P,\mathrm{exp}}$ or $k_{P,\mathrm{lin}}$. The same mathematical description applies to reactive power-to-frequency dependency with Q_0, $k_{Q,\mathrm{exp}}$ and $k_{Q,\mathrm{lin}}$.

$$P_{\mathrm{exp}}(f) = P_0 \times \left(\frac{f}{f_0}\right)^{k_{P,\mathrm{exp}}} \tag{1}$$

$$P_{\mathrm{lin}}(f) = P_0 \times \left(1 + k_{P,\mathrm{lin}} \frac{f - f_0}{f_0}\right) \tag{2}$$

The linear frequency-dependent modelling approach, which was originally derived from the exponential approach through Taylor series expansion [8], seems to be more common. The linear model is also the only one mentioned by standard literature such as Kundur (2022) [9], where model parameters both for single load devices and aggregate loads can be found. However, the data in [9] is actually based on studies conducted in the 1970s and 1980s. Power electronics have brought significant changes in load technology since then [3]. Thus, we assume those parameters to be outdated. In addition, it is unclear whether the parameters were identified with the aim to represent load behavior during larger frequency deviations of multiple hertz. A considerably wide range of 60±6 Hz was considered by the authors of [10], who presented experimental results in 1998. However, only different types of fluorescent light and the composite load of office equipment were included in the study. Similar to our approach (see Section 3.2), the authors identified parameters for the linear model by exposing the loads to steady-state frequency deviations. In contrast to our study, however, it was not verified whether the identified models can be used to reconstruct the real load behavior during dynamic frequency variations.

3 Methodology

This section explains the experimental procedure followed to obtain the results presented in Section 4.

3.1 Devices under test, setup and measuring equipment

To minimize the impact of potential internal state changes on the active and reactive power consumption, we selected simple on-off devices with supposedly constant load behavior. The three single-phase devices under test are shown in Fig. 1 (right), along with the corresponding brand, model and the tested operating mode. The selected devices use representative technologies that are commonly seen in low-voltage loads [2]:

- Halogen floodlight ***(H)***: a representative of resistive loads.
- LED floodlight ***(L)***: a representative of power electronic-interfaced loads. The device exhibits a capacitive behavior.
- Floor fan ***(F)***: a representative of directly connected motor loads. Two of the three available power levels were tested. The fan exhibits a capacitive behavior in power level 1 (***F*^{1}**), and an inductive behavior in power level 3 (***F*^{3}**).

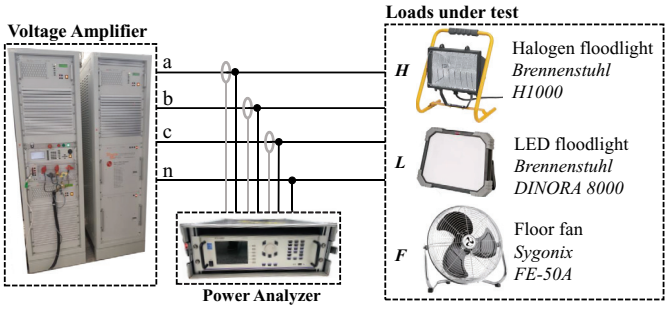

Fig. 1. Experimental setup with devices under test

As illustrated in Fig. 1, one device per phase at a time was connected to a four-quadrant voltage amplifier. This allows for the exposure of the loads to artificial grid frequency fluctuations in the range 44–56 Hz, while the phase voltage is maintained at the nominal value of 230 V. To measure the active and reactive power consumption of the loads, we used the power analyzer LMG500 by ZES Zimmer and corresponding current clamps. The measurement cycle time was 50 ms.

3.2 Steady-state tests for static model generation

In Fig. 2, our measurement-based approach is illustrated by the example of the active power consumption of the fan (level 1). We followed the same procedure for reactive power.

First, the devices were exposed to steady-state frequency deviations in steps of 1 Hz, with a duration of 90 s each. The devices were turned off when changing from one steady-state deviation step to another. To minimize the impact of startup behavior, we used the measurement data from the last 30 s—visualized as boxplots in Fig. 2 (left)—to calculate the average steady-state power consumption values $P_{\mathrm{meas},\varnothing}(f)$ for each frequency step f. It should be remarked that all power values are displayed in per unit (p.u.). We used $P_{\mathrm{meas},\varnothing}(50\,\mathrm{Hz}) = P_0$ as base power value for normalization. Based on the measured power under various frequency values $P_{\mathrm{meas},\varnothing}(f)$, we identified the following three different static models:

- **Lookup table model:** Linear interpolation in between the $P_{\mathrm{meas},\varnothing}(f)$ values; gray line in Fig. 2 (left).
- **Exponential model:** Curve fit, i.e. least-squares approximation, of (1) to $P_{\mathrm{meas},\varnothing}(f)$; green dotted line.
- **Linear model:** Curve fit of (2) to $P_{\mathrm{meas},\varnothing}(f)$; green dashed line.

For the linear and the exponential model, the goodness of fit was quantified by the sum of squared errors (SSE). This is outlined in (3) by the example of the exponential $P(f)$ model. In Fig. 2 (left), the error $\Delta P\,(f = 45\,\mathrm{Hz})$ is marked in red.

$$\mathrm{SSE}_{P,\mathrm{exp}} = \sum_{f=44\,\mathrm{Hz}}^{f=56\,\mathrm{Hz}} \Big(\underbrace{P_{\mathrm{meas},\varnothing}(f) - P_{\mathrm{exp}}(f)}_{\Delta P(f)}\Big)^2 \ (\mathrm{p.u.}^2) \tag{3}$$

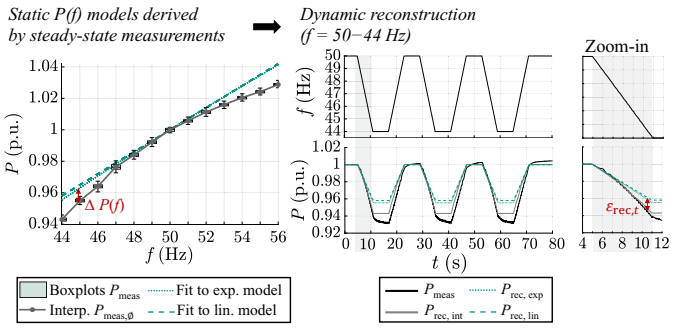

Fig. 2. Explanation of the methodology by the example of $\boldsymbol{F^1}$

3.3 Dynamic tests and evaluation of the reconstruction error

To test whether the static models identified according to Section 3.2 can be used to reconstruct the power during dynamic frequency variations, we exposed the devices to dynamic trapezoidal disturbances in the range 50–44 Hz (underfrequency tests) and 50–56 Hz (overfrequency tests). The rate-of-change-of-frequency (RoCoF) of the ramps varied among ±0.5 Hz/s, ±1 Hz/s and ±2 Hz/s. Fig. 2 (middle) illustrates the example of the 1 Hz/s underfrequency test. To verify whether the overall frequency-dependent performance of the devices is consistent, each type of trapezoidal disturbance was repeated three times. In the following, the data processing procedure will be described for active power. It should be noticed that the same procedure was followed for reactive power.

It was observed that the same device does not necessarily consume exactly the same power at 50 Hz during different tests. Hence, to compare the measured power (black line in Fig. 2) to the reconstructed power (gray and green lines), the measured power was normalized by P_0^*, and the reconstructed power was normalized by P_0. P_0^* was calculated by averaging the values of the five seconds before the first ramp starts. In the case of our devices and scenarios under test, the largest discrepancies were found for $\boldsymbol{F^1}$: 1.6 % (1.9 W) for P_0^* compared to P_0, and 3.0 % (0.7 var) for Q_0^* compared to Q_0.

At each sample time t, the absolute reconstruction error $e_{\mathrm{rec},t}$ can be calculated from (4), where $P_{\mathrm{rec},t}$ is the reconstructed power and $P_{\mathrm{meas},t}$ is the measured power. For instance, the linear model error $e_{\mathrm{rec},10.5\,\mathrm{s}}$ is marked in red in Fig. 2 (zoom-in, bottom).

$$e_{\mathrm{rec},t} = |P_{\mathrm{rec},t} - P_{\mathrm{meas},t}| \quad \text{(p.u.)} \tag{4}$$

For a quantitative evaluation of the reconstruction error, we used the data from the first ramp of the first trapezoidal to obtain the average absolute error value $e_{\mathrm{rec},\varnothing}$. The corresponding data range is marked in gray in Fig. 2.

4 Overview and Discussion of the Results

In this section, we describe and discuss the results. It should be remarked that in case of the halogen floodlight (***H***), we only considered the active power consumption. The power factor of this device is approximately 1, which inhibits an accurate measurement of the reactive power consumption.

Table 1 Model parameters and goodness of curve fit (SSE)

	P_0	$k_{P,\mathrm{exp}}$	$k_{P,\mathrm{lin}}$	$\mathrm{SSE}_{P,\mathrm{exp}}$	$\mathrm{SSE}_{P,\mathrm{lin}}$
H	742 W	0.00	0.00	3×10^{-6} p.u.^{2}	3×10^{-6} p.u.^{2}
L	66 W	–0.07	–0.07	$\mathbf{1\times10^{-5}}$ **p.u.^{2}**	2×10^{-5} p.u.^{2}
F^1	114 W	0.36	0.35	$\mathbf{6\times10^{-4}}$ **p.u.^{2}**	8×10^{-4} p.u.^{2}
F^3	141 W	0.62	0.66	0.009 p.u.^{2}	**0.008 p.u.^{2}**
	Q_0	$k_{Q,\mathrm{exp}}$	$k_{Q,\mathrm{lin}}$	$\mathrm{SSE}_{Q,\mathrm{exp}}$	$\mathrm{SSE}_{Q,\mathrm{lin}}$
H	0 var*	–	–	–	–
L	15 var	0.54	0.55	1×10^{-4} p.u.^{2}	$\mathbf{8\times10^{-5}}$ **p.u.^{2}**
F^1	23 var	2.40	2.24	0.024 p.u.^{2}	**0.011 p.u.^{2}**
F^3	27 var	–3.81	–3.94	**0.004 p.u.^{2}**	0.048 p.u.^{2}

*Low measurement accuracy, thus neglected in our analysis.

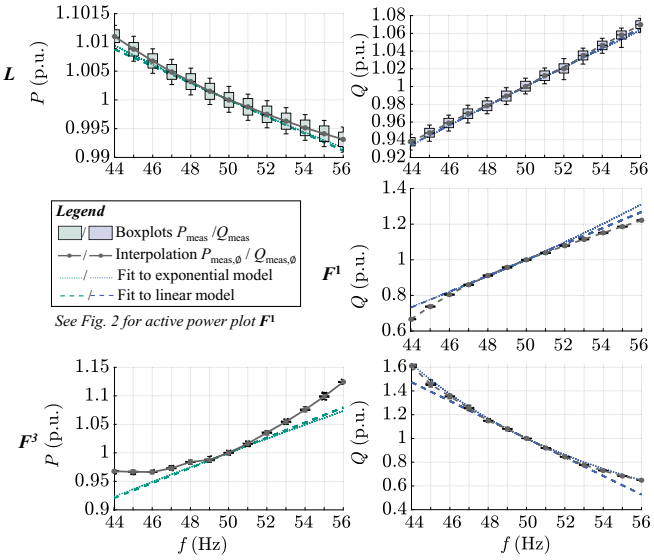

Fig. 3 Measured steady-state $P(f)$ behavior (left) and $Q(f)$ behavior (right), together with derived static models

4.1 Steady-state power-to-frequency dependency

Table 1 lists the reference values P_0 and Q_0, i.e. the average active and reactive power measured at 50 Hz (see Section 3.2), for each device. In addition, the parameters identified for the exponential and linear model are presented together with the corresponding goodness of fit values. The smaller value, i.e. the better fit result, is written in bold font.

As to be expected for resistive loads, ***H*** does not show any remarkable frequency dependency in its active power consumption. Thus, $k_{P,\mathrm{exp}}$ and $k_{P,\mathrm{lin}}$ were identified to be zero.

Fig. 3 presents the measured steady-state power at discrete frequency steps (boxplots) of ***L*** and ***F*** (both levels $\boldsymbol{F^1}$ and $\boldsymbol{F^3}$). For those devices, we determined model parameters greater or lower than zero. Since all power values are displayed in per unit, one can get a preliminary understanding of the variations in steady-state power-to-frequency dependency by examining the extension of the y-axis. In general, a larger extension of the y-axis is also reflected in higher absolute model parameters. The largest absolute parameter

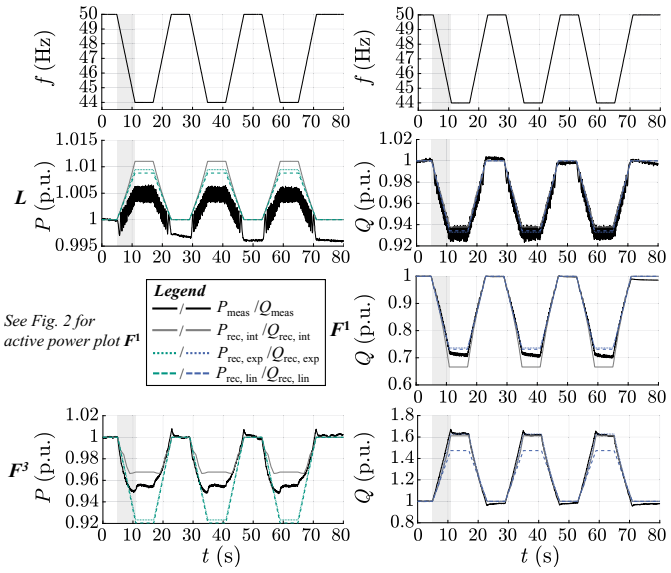

Fig. 4 Comparison of measured and reconstructed active power (left) and reactive power (right) during underfrequency test with RoCoF of 1 Hz/s

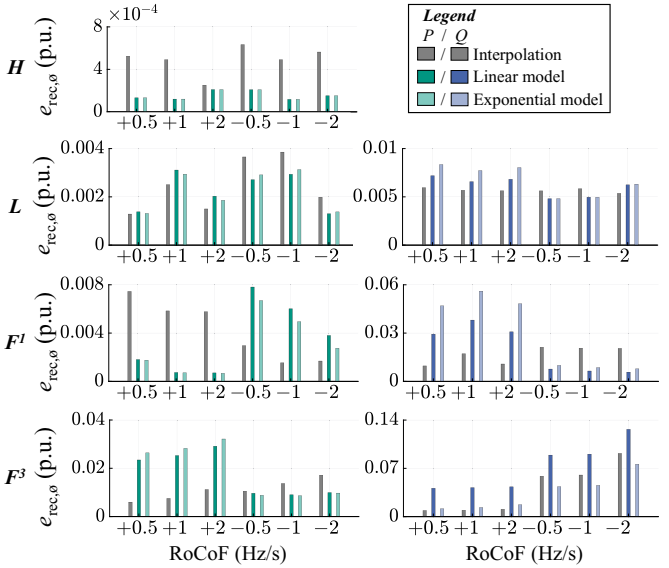

Fig. 5 Comparison of mean absolute reconstruction errors for active power (left) and reactive power (right)

is $k_{Q,\mathrm{exp}} = -3.94$ for $\boldsymbol{F^3}$, which—as to be expected for the only device (level) with inductive behavior—shows a negative reactive power-to-frequency relationship.

When comparing the fit results for the exponential and linear model (see Table 1), the most remarkable difference can be observed for the reactive power consumption of $\boldsymbol{F^3}$, where $\mathrm{SSE}_{Q,\mathrm{exp}}$ is approximately 10 times lower than $\mathrm{SSE}_{Q,\mathrm{lin}}$. However, although the active power boxplots of $\boldsymbol{F^3}$ also suggest an exponential active power-to-frequency relationship, the measured behavior cannot be accurately reproduced by a single-parameter exponential model as formulated in (1). Here, $\mathrm{SSE}_{P,\mathrm{lin}}$ is even 0.001 p.u.^{2} smaller than $\mathrm{SSE}_{P,\mathrm{exp}}$.

4.2 Reconstruction during dynamic disturbances

Fig. 4 shows the measured and reconstructed active power (left) and reactive power (right) during the dynamic 1 Hz/s underfrequency test scenario for devices $\boldsymbol{L}$ and $\boldsymbol{F}$ (both tested levels). Fig. 5 outlines the average absolute reconstruction error value $e_{\mathrm{rec},\varnothing}$ for all devices and scenarios under test. Since only the first ramp was considered for the calculation of $e_{\mathrm{rec},\varnothing}$ (see Section 3.3), negative RoCoF values refer to underfrequency tests, whereas positive ones refer to overfrequency tests. As an initial observation, we can state that the comparison of error values from different test scenarios does not allow us to draw any general conclusions with respect to the impact of RoCoF magnitude or sign on the reconstruction error.

The plots in Fig. 5 suggest that the lookup table model, i.e. the linear interpolation in between average steady-state power values, manages to reconstruct general patterns in dynamic frequency-dependent power characteristics. For instance, in the steady-state measurements (interpolation shown as gray line in Fig. 4) of $\boldsymbol{F^3}$, active power can be observed to gradually decline with decreasing frequency in the range 46–50 Hz, but to slightly increase in the range 44–46 Hz ($t = 10$–11 s). The measured dynamic power response (black line) exhibits consistent behavior. However, e.g. in case of the $Q(f)$ behavior of $\boldsymbol{F^1}$, the reconstruction based on interpolation tends to overestimate the dynamic power response. Here, the exponential and linear model show a better reconstruction performance, which is confirmed by the respective error bars (Fig. 5, 3rd row, right).

The overall smallest error values of below 0.0007 p.u.—most likely attributable to measurement inaccuracy—were calculated for $\boldsymbol{H}$. This confirms that frequency dependency of this resistive device is negligibly small compared to the other devices, both in steady state and during dynamic disturbances.

For the device $\boldsymbol{L}$, the reconstruction error remained below 0.008 p.u. in all scenarios. It should be noted that the decrease of frequency from 50 to 44 Hz resulted in a reactive power decrease by approximately 0.08 p.u. (see Fig. 3 and Fig. 4), while changes in active power were only around 0.01 p.u. This suggests that the reactive power-to-frequency-dependency of power electronic-interfaced loads is much larger than active power-to-frequency dependency.

The largest reconstruction errors of approximately 0.13 p.u. (see Fig. 5, 4th row, right) were calculated for $\boldsymbol{F}$. It has already been shown in other studies that static load models tend to be less accurate for motor-based loads during dynamic voltage fluctuations [2]. It is thus not surprising that we can observe a similar phenomenon for frequency variations.

5 Conclusion and Outlook

In this paper, we presented an experimental investigation into the frequency-dependent power characteristics of low-voltage loads. The three selected devices under test are representative of frequently employed load technologies in low-voltage grids. First, the loads were exposed to steady-state frequency deviations in the range 50±6 Hz with steps of 1 Hz difference. For

active and reactive power of each device, the measured average power at each step was used to identify three static load models; a lookup table model based on interpolation, as well as an exponential model and a linear model based on curve fitting. These models were used to reconstruct the power during dynamic trapezoidal frequency variations. When we compared the real measured power during the dynamic tests to the reconstructed power, we noticed that the largest mean discrepancy of approximately 0.13 p.u. occurs for the fan, a motor-based load. For the LED floodlight, a power electronic-interfaced load, we observed that reactive power exhibits significantly more frequency dependency than active power. During both the steady-state and the dynamic tests, a frequency decrease to 44 Hz led to a decline in reactive power by 0.08 p.u. It may be important to consider this behavior in studies of future distribution grid scenarios, since the share of this load technology can be expected to further grow in the future. The results presented in our study can also be applied to novel demand-side management strategies such as frequency-based power control [5, 6].

6 Acknowledgments

This work was supported by the Helmholtz Association under the Program "Energy System Design" and under the Helmholtz Young Investigator Group "Hybrid Networks" (VH-NG-1613).

7 References

[1] Milanović, J. V., Yamashita, K., Martínez Villanueva, S., et al.: 'International Industry Practice on Power System Load Modeling', IEEE Transactions on Power Systems, 2013, 28, (3), pp. 3038–3046

[2] WG C4.605, 'Modelling and aggregation of loads in flexible power networks' (CIGRE, 2014)

[3] Korunović, L. M., Milanović, J. V., Djokic, S. Z., et al.: 'Recommended parameter values and ranges of most frequently used static load models', IEEE Transactions on Power Systems, 2018, 33, (6), pp. 5923–5934

[4] SPD – Inertia TF, 'Inertia and Rate of Change of Frequency (RoCoF) - Version 17' (ENTSO-E, 2020)

[5] Tao, Q., Geis-Schroer, J., Wald, F., et al.: 'The Potential of Frequency-Based Power Control in Distribution Grids'. IEEE 13th International Symposium on Power Electronics for Distributed Generation Systems (PEDG), Kiel, Germany, June 2022, pp. 1–6

[6] Wald, F., Tao, Q., Carne, G. D.: 'Virtual Synchronous Machine Control for Asynchronous Grid Connections', IEEE Transactions on Power Delivery, 2023, 39, (1), pp. 397–406

[7] Geis-Schroer, J., Suriyah, M., Leibfried, T.: 'Frequency Fluctuations in European Isolated Systems: A Review on Standards, Available Recordings and Grid Code Requirements'. 58th Int. Universities Power Engineering Conference (UPEC), Dublin, Ireland, August 2023, pp. 1–6

[8] Schulz, R. P., Turner, A. E., Ewart, D. N.: 'Long term power system dynamics. Volume I. Summary and technical report', 1974

[9] Kundur, P., Balu, N. J.: 'Power System Stability and Control' (McGraw-Hill, 2022, 2nd edn. 2022)

[10] Hajagos, L. M., Danai, B.: 'Laboratory measurements and models of modern loads and their effect on voltage stability studies', IEEE Transactions on Power Systems, 1998, 13, (2), pp. 584-592